Rare Metal Materials and Engineering
Volume 50, Issue 1, January 2021
Available online at www.rmme.ac.cn

Science Press

Cite this article as: Rare Metal Materials and Engineering, 2021, 50(1): 0095-0101.

ARTICLE

Microstructure and Mechanical Properties of an Al-Cu-Sn Wall Deposited by Wire + Arc Additive Manufacturing

Wang Shuai[1], Gu Huimin[1], Wang Wei[2], Li Chengde[1], Ren Lingling[1], Wang Zhenbiao[3], Zhai Yuchun[1,3], Ma Peihua[1]

[1] College of Metallurgy, Northeastern University, Shenyang 110819, China; [2] Inner Mongolia Metal Material Research Institute, Inner Mongolia 014000, China; [3] Fushun Dong gong Metallurgical Materials and Technology Limited Company, Fushun 113000, China

Abstract: The Al-Cu alloy walls (ZL205A) produced by wire + arc additive manufacturing (WAAM) have good mechanical properties, but toxic cadmium oxide is generated during production. Therefore, to prevent the generation of cadmium oxide, Cd was replaced by Sn in the Al-Cu alloy (ZL205A) in the present paper. The microstructure and mechanical properties of Al-Cu-Sn alloy and the ZL205A alloy walls in as-deposited and T6 state were investigated and compared by conducting metallographic, scanning electron microscopy, energy dispersive spectroscopy, transmission electron microscopy, and tensile tests. The surface of the Al-Cu-Sn alloy wall is smooth and exhibits a silver-white luster, and the burning loss rate of Sn is 5.9%. The grains of the WAAM Al-Cu-Sn alloy wall are fine and uniform, which are smaller than these of the ZL205A alloy wall. The main precipitated phases are uniformly distributed among the grains or on the grain boundaries. Following T6 heat treatment, the θ phases are completely dissolved in the Al matrix, and the re-melted T phases and small co-phases of Sn and Al_2Cu are uniformly distributed on the grain boundaries. The TEM results show that a large number of θ' phases are dispersed among the grains. The mechanical properties of the Al-Cu-Sn alloy after heat treatment are as follows: tensile strength 493 MPa, yield strength 434 MPa, and elongation rate 9.5%. The alloy shows excellent performance in WAAM process and has broad application prospects.

Key words: Al-Cu-Sn alloy; wire + arc additive manufacturing (WAAM); microstructure; mechanical property

Al-Cu alloys are known as hard aluminum alloys because of their high strength, and are widely used in aerospace[1,2]. These alloys can be categorized as casting or deformation alloys, based on their formation method. During the casting of Al-Cu alloys, segregation[3] and thermal cracking[4,5] easily occur, and shrinkage cavities and pores[6] form as a wide range of crystallization temperatures are used, which result in the low yield of poor-quality alloys. Deformation Al-Cu alloys are heat-treatable and strengthened; however, it is difficult to match the strength of their weld seams with that of the base material. These factors significantly limit the application of Al-Cu alloys.

Metallic structural components prepared through wire + arc additive manufacturing (WAAM) have a high product density[7] and good internal quality[8], and this process conserves materials[9] and has a short production cycle[10]. The raw material is the main hindrance to the application of this technology in the production of Al-Cu alloys. Gu et al.[11] used deformation Al-Cu alloy 2219 as a raw material and found that T6 heat treatment provided the wall with high tensile strength (470 MPa) and elongation rate (17%), but resulted in low yield strength (300 MPa). Qi et al.[12,13] used Al-Cu-Mg alloy as the raw material for WAAM to investigate the properties of the deposition body, and also faced the issue of a low yield strength. Wang et al.[14] used casting Al-Cu alloy ZL205A as a raw material and found that the wall produced with T6 heat treatment had good mechanical properties, with a tensile strength of 500 MPa, yield strength of 450 MPa, and elongation rate of 10%, and the horizontal and longitudinal mechanical properties of the

Received date: January 10, 2020
Foundation item: National Key R&D Program of China (2018YFB1106300-5)
Corresponding author: Gu Huimin, Ph. D., College of Metallurgy, Northeastern University, Shenyang 110819, P. R. China, E-mail: guhm@smm.neu.edu.cn

deposition body were consistent. However, Zl205A alloy contains Cd, which severely burns under the action of an arc, and a layer of toxic yellow-brown cadmium oxide forms on the surface of the wall. This Al-Cu alloy cannot be used in industry. Therefore, it is urgent that we develop a high-strength and tough Al-Cu alloy suitable for wire arc additive manufacturing.

In an Al matrix, Cd has low solid solubility, a high diffusion rate, and forms strong bonds with the vacancies in the solution. Therefore, during the heat treatment of Al-Cu alloys, Cd precipitates quickly and binds with the vacancies produced in the solid solution, inhibiting the formation of a GP area and improving the nucleation rate of the strengthening phase. This can shorten the Al-Cu alloy formation period and improve the peak intensity of aging. They also found that Sn and In play the same role as Cd in Al-Cu alloy[15-17]. Sn has more industrial application prospects as it is cheaper than In. Furthermore, the boiling point (2602 ºC) of Sn is higher than that of Cd (767 ºC). Therefore, using Sn in the alloy smelting and WAAM will result in a lower element loss rate.

In this study, we replaced Cd with Sn in a base ZL205A alloy. The microstructure and mechanical properties of the Al-Cu-Sn alloy wall produced by WAAM were investigated to explore the production of a suitable Al-Cu alloy for undergoing the WAAM process with high-strength and toughness.

1 Experiment

The Al-Cu-Sn alloy welding wire used in this experiment was produced by North East Industrial Materials & Metallurgy Co., Ltd, and had a diameter of 1.2 mm. The main alloy elements and impurities of the welding wire are shown in Table 1. A 10 mm 2219 aluminum plate purchased from Dong Qing was used as the base plate in the additive process.

The additive manufacturing system is shown in Fig.1a. The system includes a Fronius Advance 4000 arc welding power supply and an ABB 1410 welding robot. The additive manufacturing process is shown in Fig. 1b, and the dimensions of the wall are 200 mm×150 mm with 53 layers. The *x*-axis corresponds to the front of the wall, the *y*-axis corresponds to the heat source movement direction, horizontal along the wall, and the *z*-axis corresponds to the direction of growth, perpendicular to the wall.

The print parameters are shown in Table 2, where *I* is the welding current, *U* is the welding voltage, v_{WFS} is the wire feeding speed, and v_{TS} is the torch traveling speed. The wall was heat-treated at a solution temperature of 535 ºC for 360 min with a quenching water temperature of 40 ºC, and aged at 180 ºC for 120 min, which are the common heat treatment parameters for ZL205A alloy .

The chemical composition of the wall was tested using an OXFORD EDM direct reading spectrometer, while the mechanical properties were tested using a WDW-300 mi cro-controlled electronic universal testing machine. The microstructure and morphology were observed using a

Table 1 Chemical composition of the raw material (wt%)

Element	Fe	Si	Mg	Cu	Mn	Ti	Sn	Zr	B	V
Content	0.100	0.040	0.025	5.102	0.421	0.272	0.103	0.177	0.034	0.125

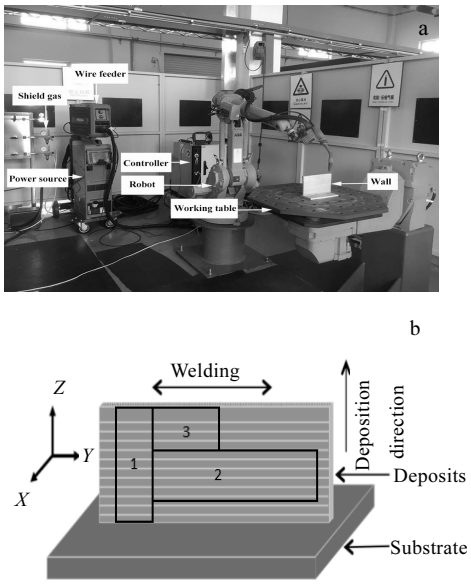

Fig.1 Additive manufacturing system (a) and wall sampling location (b)

Table 2 Print parameters

I/A	*U*/V	v_{WFS}/m·min^{-1}	v_{TS}/mm·s^{-1}	Cooling time/s
98	11.2	6.5	8	60

LEICA MEF4M metallographic microscope and a QUANTA FEG 250 scanning electron microscope (SEM), and element and phase analyses were conducted by energy dispersive spectroscopy (EDS). The morphology of precipitated phase was observed using a spheroidal transmission electron microscope (TEM). The sampling position and shape of the mechanical sample are also shown in Fig.1b. Tensile samples were captured at positions 1 and 2, and metallographic and transmission samples were captured at position 3. The tensile sample was fabricated into a plate with a standard distance of 30 mm and cross-sectional area of 2.5 mm×10 mm.

2 Results and Discussion

2.1 Surface morphology and chemical composition

The surface morphologies of the Al-Cu-Sn and ZL205A alloy walls are shown in Fig.2. The surfaces of both walls

were flat, and there were uniform contours generated by the accumulation of layers. The surface of the Al-Cu-Sn alloy wall was silver-white, as shown in Fig.2a, while that of the ZL205A alloy was covered with yellow-brown powder, asshown in Fig.2b. This is due to the toxic metal oxides produced by the burning of Cd[14].

The chemical composition and element burning loss rate of the Al-Cu-Sn alloy wall are shown in Table 3. During WAAM, the content of impurities in the wall, such as Fe and Si, increased and the burning loss rate of B was highest, reaching 55.8%. The burning loss rates of other elements were all below 10%. All elements could meet the requirements of the ZL205A standard, excluding Sn, which had a burning loss rate of 5.9%. This was much lower than that of Cd (50%). Therefore, it is easier to control the chemical composition of products containing Al-Cu-Sn alloys than that of those containing ZL205A.

2.2 Microstructure

2.2.1 As-deposited microstructure

The microstructure of the as-deposited Al-Cu-Sn and ZL205A alloy walls are shown in Fig.3. No pores could be seen in the microstructures of the walls of both alloys. First, during the WAAM process, the transition and solidification of each drop of the alloy liquid occurred under the protection of high-purity Ar, which stopped air and reduced the possibility of the generation of shrinkage defects. Second, both alloys were composed of cast aluminum with good fluidity. Therefore, the feeding ability was strong in the solidification process, and the tendency to produce shrinkage cavities was low. Finally, during WAAM, the lower layers could be re-melted by the subsequent layers, which was beneficial for removing defects. In addition, CMT-PADV (CMT+Pulse+ Advance) process can control the porosity efficiently due to the low heat input, a fine equiaxed grain structure and effective oxide cleaning of the wire[18].

Thanks to the high cooling speed and stirring effect of the arc on the molten pool, the grains in the walls of the two alloys formed by WAAM were uniform and consisted of fine isometric crystals. Fig.3a shows that the grain size of the as-deposited Al-Cu-Sn alloy wall is smaller and more uniform than that of ZL205A alloy shown in Fig.3b. The addition of Sn tended to refine the grains of the Al substrate because its solubility in Al is low. The solidification was likely to segregate at the grain boundary, which would increase the size of the constitutionally supercooled zone and the number of nucleation sites. This also inhibited the migration of the interface during solidification and hindered the growth of α-Al, thereby refining the grains[19]. Sn has a smaller solid solubility in Al than Cd, and it precipitates at the interface more easily during solidification, which increases the size of the supercooling zone of components and produces finer grains.

Table 3 Chemical composition and element burning loss rate of Al-Cu-Sn alloy wall

Element	Fe	Si	Mg	Cu	Mn	Ti	Sn	Zr	B	V
Content/wt%	0.110	0.044	0.023	4.855	0.404	0.255	0.097	0.162	0.015	0.120
Burn-out rate/%	-10	-10	8	4.8	4.0	6.5	5.9	8.5	55.8	4

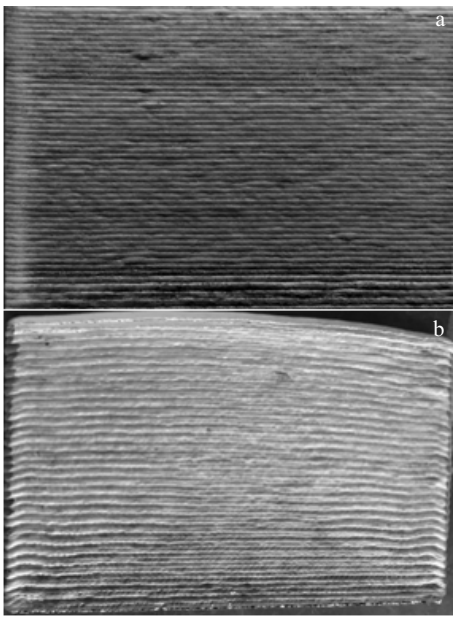

Fig.2 Surface morphologies of walls: (a) Al-Cu-Sn alloy and (b) ZL205A alloy

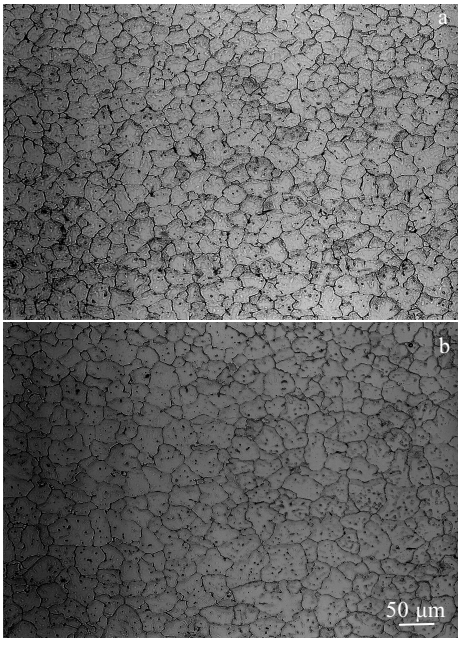

Fig.3 Microstructures of the as-deposited Al-Cu-Sn (a) and ZL205A alloy walls (b)

Fig.3 shows that the precipitated phases of the two types of alloys wall exhibit no clear segregation phenomena and are uniformly distributed among the grains or on the grain boundaries. The SEM and EDS results of the Al-Cu-Sn alloy walls are shown in Fig 4. The EDS analysis results show that θ (Al_2Cu) and T ($Al_{12}Mn_2Cu$) are the main precipitated phases of the wall, and the main precipitated phases are consistent with those of a ZL205A alloy wall[14]. In the Al-Cu-Sn alloy wall, the θ phase mainly exhibited a network morphology, with a small amount of slender strips, and the morphology of the precipitated phase was consistent with that of the ZL205A alloy. This morphology has a large contact area with the matrix; hence, so it is easier for the metal to dissolve in the matrix during solution treatment.

2.2.2 Microstructure after T6 treatment

The microstructures of the walls of the Al-Cu-Sn and ZL205A alloys in the T6 state are shown in Fig.5. As shown in Fig.5a, after heat treatment, there are pores on the Al-Cu-Sn alloy wall, which were caused by the diffusion and convergence of smaller pores during solution treatment. The ZL205A alloy wall also exhibit this type of defect, as shown in Fig.5b. Following T6 treatment, the grains of the Al-Cu-Sn alloy wall were still fine and existed as uniform isometric crystals, and their grain size is the same as that in the as-deposited state. The grain size of the Al-Cu-Sn alloy wall was still slightly smaller than that of the ZL205A alloy wall after T6 heat treatment, due to the genetic effect of the alloy.

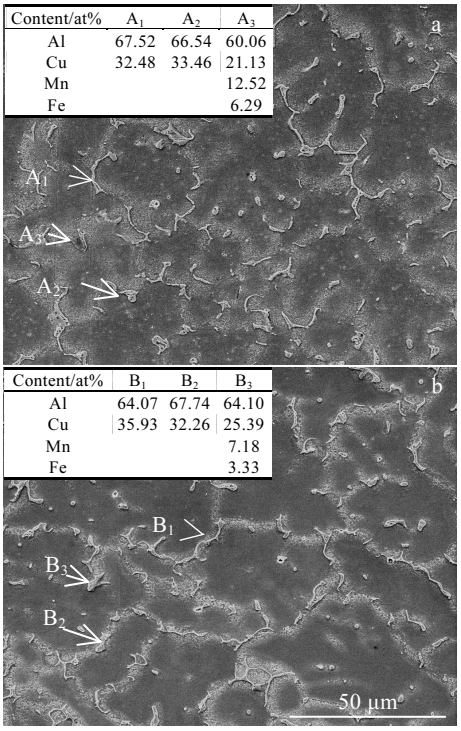

Fig.4 SEM and EDS results of the as-deposited Al-Cu-Sn (a) and ZL205A alloy walls (b)

Following heat treatment, the as-deposited precipitated θ phases (Al_2Cu) exhibiting network and long strip morphologies were dissolved in the Al matrix, and uniformly precipitated among the grains or on the grain boundaries during aging. By comparing Fig.5a and 5b, the amount of the precipitated θ phase on the grain boundaries in the Al-Cu-Sn alloy wall was higher than that in the ZL205A alloy wall. The SEM and EDS analyses of the Al-Cu-Sn alloy wall presented in Fig. 6 show that the precipitated phases after heat treat

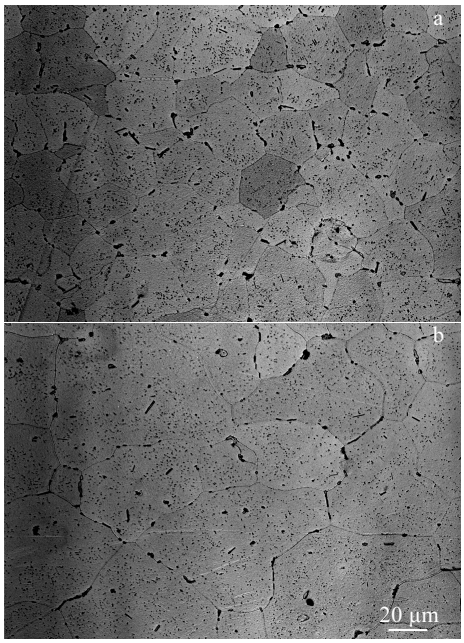

Fig.5 Microstructures of the T6-treated Al-Cu-Sn (a) and ZL205A alloy walls (b)

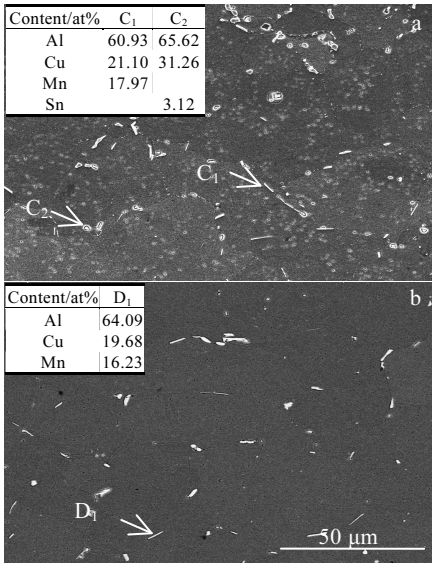

Fig.6 SEM and EDS results of the Al-Cu-Sn (a) and ZL205A alloy walls (b) in the T6 state

ment mainly consist of the re-melted T-phase with a small amount of Fe, as indicated by C1 in Fig. 6a, and the θ phase, which is associated with Sn, is indicated as C2 in Fig. 6a. As the θ phase was not observed on the microstructure of the as-deposited wall, this phase likely precipitated during the aging process. Following T6 treatment, the precipitated phase of the ZL205A alloy wall only consists of the T-phase, as shown in Fig. 6b. The precipitation sequence of Al-Cu alloys during aging is as follows [20]: supersaturated solid solution (α ss) > GP zone > (GP Ⅰ) > θ''(GP Ⅱ) > θ'> θ. The addition of Sn accelerated the aging of Al-Cu alloys under the heat treatment system described here, as the Sn particles grew. Part of the transition phase surrounding the Sn particles expanded into equilibrium phase with a size smaller than 5 μm and diffused along the grain boundaries. The dispersion of the precipitated phase along the grain boundaries lead to a nail-rolling effect, which aids in preventing the material from plastic deformation.

2.2.3 Transition phase morphology

The TEM images of the Al-Cu-Sn and ZL205A alloy walls in the peak aging states are shown in Fig. 7. As shown in Fig. 7a, the Al-Cu-Sn alloy wall contains three types of precipitates in its peak aging state, including two rod-like precipitates facing in different directions and one flake-like precipitate, all of which contain the θ' phase, as indicated by E_1, E_2, and E_3[21]. Due to the different incident angles, the walls contained different forms of θ', including elliptic sheet materials with a length, width, and thickness of 100, 50, and 5 nm, respectively. The TEM images of the ZL205A alloy wall in the peak aging state also exhibit three forms of θ' phase, as shown in Fig. 7b. The size and distribution of the θ' phases in the Al-Cu-Sn alloy wall are consistent with those of the ZL205A alloy. However, the spaces between the precipitation phases are slightly larger. This is because the T6-treated Al-Cu-Sn alloy wall include some θ' phases, which grew to form the θ equilibrium phase. Therefore, it can be concluded that Sn plays the same role as Cd in the aging of WAAM Al-Cu alloy walls. Sn has a high diffusion coefficient in an aluminum matrix. Therefore, during the early aging stage, the solute Sn atoms are biased to form Sn-Sn clusters, which reduces the mismatch between θ' nucleation points and the aluminum matrix, thereby promoting nucleation[22].

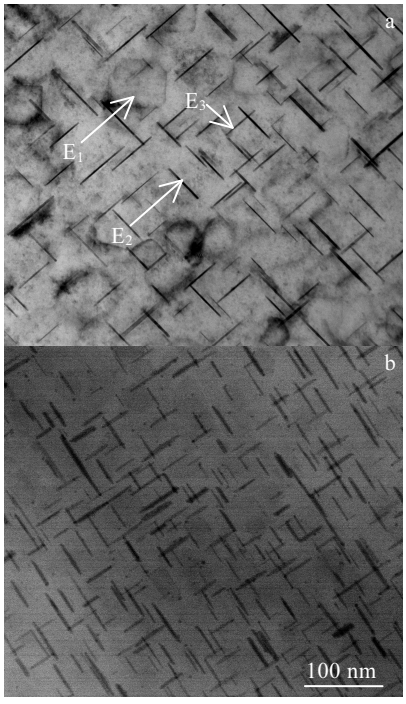

Fig.7 TEM images of the T6-treated Al-Cu-Sn (a) and ZL205A alloy walls (b)

2.3 Mechanical properties and fracture morphology

2.3.1 Mechanical properties

The mechanical properties of the Al-Cu-Sn and ZL205A alloy walls in the T6 state are shown in Fig. 8. The mechanical properties of Al-Cu-Sn alloy are as follows: tensile strength 493 MPa, yield strength 434 MPa, and elongation rate 9.5%. This yield strength is much higher than that of 2219 (300 MPa)[11] and 2024 (320 MPa)[12].The tensile strength and elongation rate are close to those of the ZL205A alloy wall, while the yield strength is 16 MPa lower. This is mainly because, during the aging process, some of the θ' phase transformed into the θ equilibrium phase, resulting in an increase in the space between the θ' phases and resulting in a slight decrease in the yield strength.

2.3.2 Fracture morphology

The fracture morphologies of the Al-Cu-Sn and ZL205A alloy walls in the T6 state are shown in Fig.9. Fig.9a shows that ductile fractures form on the Al-Cu-Sn alloy wall, and numerous dimples are homogeneously distributed throughout the fracture, indicating that the alloy has good toughness. The size and distribution of dimples in the Al-Cu-Sn alloy wall were consistent with those of the ZL205A alloy wall. However, more of the precipitated phase formed at the base of the dimples in the Al-Cu-Sn alloy than the ZL205A alloy, indicating that more precipitated phases were distributed on the grain boundaries in the microstructure of the Al-Cu-Sn alloy wall in the T6 state.

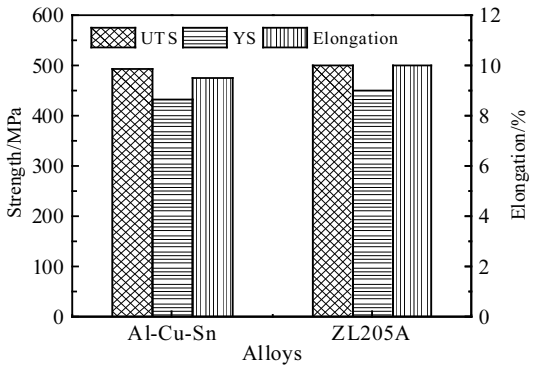

Fig.8 Mechanical properties of the Al-Cu-Sn and ZL205A alloy walls in the T6 state

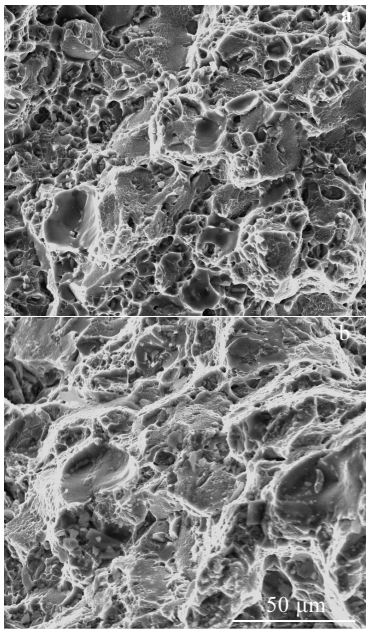

Fig.9 Fracture morphologies of the Al-Cu-Sn (a) and ZL205A alloy walls (b) in the T6 state

3 Conclusions

1) An Al-Cu-Sn wall is prepared by the WAAM process. Sn has the function of refining grains. The grain size of the WAAM Al-Cu-Sn alloy wall in the as-deposited state is uniform, and the precipitated phase is dispersed and distributed among the grains or on the grain boundaries without any segregation.

2) After solution treatment, the θ phase is completely dissolved in the matrix. After aging, a large amount of the θ' phase is dispersed among the crystals, and Sn can promote precipitation of θ' phases.

3) Following the T6-treatment of the WAAM Al-Cu-Sn alloy wall, the tensile strength, yield strength, and elongation rate are 493 MPa, 434 MPa, and 9.5%, respectively. Therefore, the Al-Cu-Sn alloy is a high-strength and tough Al-Cu alloy material suitable for the WAAM process.

References

1 Liu J, Kulak M. *Mater Sci Forum*[J], 2000, 331-337: 127
2 Lee J, Park J, Jeong H. *Mater Lett*[J], 2018, 222: 122
3 Meza E S, Bertelli F, Goulart P R *et al*. *J Alloy Compd*[J], 2013, 561: 193
4 Farup I, Drezet J M, Rappaz M. *Acta Mater*[J], 2001, 49: 1261
5 Suyitno D, Eskin G, Katgerman L. *Mater Sci Eng A*[J], 2006, 420: 1
6 Li B, Shen Y, Hu W. *Mater Des*[J], 2011, 32: 2570
7 Cong Baoqiang, Ding Jialuo. *Rare Metal Mater Eng*[J], 2014, 43(12): 3149 (in Chinese)
8 Ayarkwa K F, Williams S W, Ding J. *Addit Manuf*[J], 2017, 18: 186
9 Dinovitzer Malcolm, Chen Xiaohu, Laliberte Jeremy *et al*. *Addit Manuf*[J], 2019, 26: 138
10 McAndrew A R, Rosales M A, Colegrove P A *et al*. *Addit Manuf*[J], 2018, 21: 340
11 Gu J L. *Mater Sci Eng A*[J], 2016, 651: 18
12 Qi Z, Cong B, Qi B *et al*. *Mater Lett*[J], 2018, 230: 275
13 Qi Z, Cong B, Qi B *et al*. *J Mater Process Tech*[J], 2018, 255: 347
14 Wang Shuai, Gu Huimin, Wang Wei *et al*. *Rare Metal Mater Eng*[J], 2019, 48(9): 2910 (in Chinese)
15 Ringer S P, Hono K, Sakurai T. *Metall Mater Trans A*[J], 1995, 26: 2207
16 Sankaren R, Larid C. *Mater Sci Eng A*[J], 1974, 14: 271
17 Honma T, Saxey D W, Ringer S P. *Mater Sci Forum*[J], 2006, 519-521: 203
18 Cong B Q, Ding J L, Stewart S W. *Inter J Adv Man Tech*[J], 2015, 76(9-12): 1593
19 Jiang R P. *The Effect of Sn Addition on Aging Properties in Al-Zn-Mg-Cu Alloys*[D]. Changsha: Central South University, 2011
20 Badin C, Marino F, Verne E. *Mater Sci Eng A*[J], 1995, 191: 185
21 Banerjee S, Robi P S, Srinivasan A *et al*. *Mater Design*[J], 2010, 31: 4007
22 Silcock J M, Flower H M. *Sci Mater*[J], 2002, 46: 389

Al-Cu-Sn 合金 WAAM 堆积体的组织与性能

王　帅[1]，顾惠敏[1]，王　伟[2]，李承德[1]，任玲玲[1]，王振飚[3]，翟玉春[1,3]，马培华[1]
(1. 东北大学 冶金学院，辽宁 沈阳 110819)
(2. 内蒙古金属材料研究所，内蒙古 包头 014000)
(3. 抚顺东工冶金材料技术有限公司，辽宁 抚顺 113000)

摘　要：Al-Cu 合金 ZL205A 电弧熔丝增材制造(WAAM)堆积体具有良好的综合力学性能，但在增材过程中产生有毒的氧化镉。本研究以 Sn 替换 Cd，通过金相、SEM、EDS、TEM 及拉伸试验，考察堆积体的微观组织和力学性能，并与 ZL205A 合金堆积体进行对比。结果发现，Al-Cu-Sn 合金堆积体表面平整，呈现出银白色光泽，Sn 元素的烧损率为 5.9%。WAAM Al-Cu-Sn 合金堆积体直接堆积态晶粒细小、均匀，晶粒尺寸约为 30 μm，小于 ZL205A 合金堆积体的晶粒尺寸，主要析出相在晶内和晶界上均匀分布。T6 热处理后，θ 相完全固溶到 Al 基体中，在晶界上均匀分布着复熔 T 相和 Sn 与 Al_2Cu 的细小共生相，TEM 显示晶内弥散分布大量的 θ'相。T6 热处理后，Al-Cu-Sn 合金的力学性能为：抗拉强度 493 MPa；屈服强度 434 MPa；延伸率 9.5%。该合金在 WAAM 过程中表现出了优异的性能，具有广泛的应用前景。

关键词：Al-Cu-Sn合金；WAAM；组织；性能

作者简介：王　帅，男，1991 年生，博士生，东北大学冶金学院，辽宁 沈阳 110819，E-mail: 1061238079@qq.com